Climate Dynamics (2002) 18: 437–453
DOI 10.1007/s00382-001-0187-7

R.C. Wajsowicz

Air–sea interaction over the Indian Ocean due to variations in the Indonesian throughflow

Received: 26 July 2000 / Accepted: 22 June 2001 / Published online: 30 November 2001

Abstract The effects of the Indonesian throughflow on the upper thermocline circulation and surface heat flux over the Indian Ocean are presented for a 3-D ocean model forced by two different monthly wind–stress climatologies, as they show interesting differences, which could have implications for long-term variability in the Indian and Australasian monsoons. The effects are determined by contrasting a control run with a run in which the throughflow is blocked by an artificial landbridge across the exit channels into the Indian Ocean. In the model forced by ECMWF wind stresses, there is little impact on the annual mean surface heat flux in the region surrounding the throughflow exit straits, whereas in the model forced by SSM/I-based wind stresses, a modest throughflow of less than 5×10^6 m^3s^{-1} over the upper 300 m induces an extra 10–50 Wm^{-2} output. In the SSM/I-forced model, there is insignificant penetration of the throughflow into the northern Indian Ocean. However, in the ECMWF-forced model, the throughflow induces a 5–10 Wm^{-2} reduction in heat input into the ocean, i.e., an effective output, over the Somali Current in the annual mean. These differences are attributed to differences in the strength and direction of the Ekman transport of the ambient flow, and the vertical structure of the transport and temperature anomalies associated with the throughflow. In both models, the throughflow induces a 5–30 Wm^{-2} increase in net output over a broad swathe of the southern Indian Ocean, and a reduction in heat output of 10–60 Wm^{-2} in a large L-shaped band around Tasmania. Effective increases in throughflow-induced net output reach up to 40 (60) Wm^{-2} over the Agulhas Current retroflection in the ECMWF (SSM/I)-forced model. Seasonal variations in the throughflow's effect on the net surface heat flux are attributed to seasonal variations in the ambient circulation of the Indian Ocean, specifically in coastal upwelling along the south Javan, west Australian, and Somalian coasts, and in the depth of convective overturning between 40°S to 50°S, and its sensing of the mean throughflow's thermal anomaly. The seasonal anomalies plus annual mean yield maximum values for the throughflow-induced net surface heat output in boreal summer. Values may exceed 40 Wm^{-2} in the southern Indian Ocean interior in both models, exceed 60 Wm^{-2} over the Agulhas retroflection and immediate vicinity of the exit channels in the SSM/I-forced model, and reach 30 Wm^{-2} over the Somali jet in the ECMWF-forced model.

R. C. Wajsowicz
Department of Meteorology,
University of Maryland,
College Park, MD 20742, USA
E-mail: roxana@atmos.umd.edu

1 Introduction

A quantitative assessment of the role of the Indonesian throughflow in the global climate remains elusive. A lack of observations of flow through the Indonesian seas has meant that the modeled structure and variability of the flow in climate studies remains the choice of the model designer. Direct observations by current meters of flow through Makassar Strait, the main pathway for the mean throughflow, were made between December 1996 and July 1998, as part of the ARLINDO program, Gordon et al. (1999). Unfortunately, their measurements provide information on the current structure, and hence transport, below 250 m only. Wajsowicz et al. (personal communication) attempted to reconstruct the current profiles over the whole depth by fitting normal vertical modes, derived from climatological buoyancy frequencies, to the partial profiles. The estimated total mean transport through Makassar Strait was 10.2 Sv $\pm$4.5 Sv with a peak-to-peak interannual variation of 8.5 Sv $\pm$3.1 Sv for the transition from the 1995/1996 La Nina to the 1997/98 El Nino. Hence, the rough heat transport estimate by Talley (1984) of 0.6 PW is of the right order of magnitude,

and an indicator of the interannual variability as well. It is a significant fraction of the mean southward heat transport across 30°S in the Indian Ocean, estimated at 1.4 PW by Hsiung (1985), and as noted by Hirst and Godfrey (1993), a significant fraction of the heat input over the equatorial Pacific Ocean.

The role of the Indonesian throughflow in the global climate had been examined in modeling studies by Hirst and Godfrey (1993) (HG hereafter) and Schneider (1998) (S98 hereafter). The former used an ocean-only GCM and the latter used coupled ocean and atmosphere GCMs. In both cases, the grid resolution was very coarse, and the throughflow effect determined by contrasting results from models in which the Indonesian archipelago permitted a large mean throughflow (17.1 Sv and 13.8 Sv respectively), and in which the archipelago was blocked. In HG, using climatological mean wind stresses and surface heat and salinity fluxes, the ocean GCM, with a realistic archipelago, was spun up to a steady state. The archipelago was then closed, and the GCM integrated to a new steady state. In S98, the mean and seasonal cycle derived from a 5-year average, starting five years after the archipelago was closed, were contrasted with 5-year segments from the last 105 years of integration of the coupled GCMs with an archipelago open between Papua New Guinea (PNG) and the Asian continent, and PNG and, somewhat unrealistically, the Australian continent. Although the impact of the throughflow was shown to have global significance in both studies, the differences were assumed much larger than likely due to interannual-to-interdecadal changes in the throughflow, and so treated with some skepticism.

In the present study, the effect of the Indonesian throughflow on the Indian Ocean is re-examined using a fine-resolution, 3-D numerical global ocean model, which was originally developed for ENSO studies, see e.g., Schopf and Loughe (1995); it is cast as a quasi-isopycnic, reduced-gravity model. A thousand-year run, or an ensemble of a hundred 10-year runs, of fine-resolution, coupled ocean-atmosphere GCMs, would require computer and manpower resources beyond the reach of most groups. The similarity of the ocean sensitivity to the presence of a throughflow in HG and S98 suggests that runs of an ocean model forced by different wind–stress products might provide a guide to the internal variability expected in a coupled run. Here, the model is forced by monthly climatological wind stresses derived from European Centre for Medium-range Weather Forecasting (ECMWF) 1000 mb winds and from Special Sensor Microwave/Imager (SSM/I)-retrieved wind speeds. A description of the model and forcing data sets are given in Sect. 2. The annual mean effect of the throughflow in the two models forced by different wind stresses is described in Sect. 3. Of particular note is that the magnitude of the effect on surface heat fluxes is similar to that found in HG and S98 indicating that it is the throughflow magnitude difference over the upper ocean rather than total depth, which is the determining factor.

The HG model did not include a seasonal cycle, and in S98, the seasonal cycle in heat flux of the model throughflow was four times smaller than that of the seasonal cycle in surface heat flux of the Indian Ocean, and so the oceanic changes in the annual cycle were due primarily to the change in mean state. The coupled model gave increased monsoonal wind stresses over the Bay of Bengal and Indonesian seas for a blocked Indonesian archipelago, but no information was given on net precipitation changes. Wajsowicz and Schopf (2001) (WS henceforth) suggest that the strength of the Indian summer monsoon, measured by total rainfall, is linked to the amount of evaporation over the southern Indian Ocean. Further, this amount is influenced by the Indonesian throughflow. The seasonal variability described in Sect. 4 emphasizes the marked difference between the ECMWF-forced and SSM/I-forced models for the net surface heat flux over the Indian Ocean found in the annual mean fields. In the ECMWF-forced model, the throughflow produced increased latent heat flux over the Somali jet in boreal summer, whereas in the SSM/I-forced model, the increase occurs along the Indonesian coast to the south of Lombok Strait. Both models show a significant increase in latent heat flux over the central southern Indian Ocean, which WS note incorporates the path of the airflow heading for the Indian sub-continent. The reasons for these differences are examined in Sects. 3 and 4. A summary and discussion is given in Sect. 5.

2 Description of numerical model and experiments

2.1 The numerical model

The model is global extending from 70°S to 65°N, and is based on the POSEIDON model developed for ENSO studies, see Schopf and Loughe (1995), and Schopf (1994). It is a thermodynamic, reduced-gravity model with a generalised vertical co-ordinate. There are 14 independent layers in the vertical with 10 typically spanning the top 300 m in the tropics, and the horizontal resolution is 1°×1°, which reduces to 1°×1/3° within 15° of the equator. There is an explicit Krauss–Turner mixed layer. Vertical mixing is via a Richardson-number dependent scheme, and horizontal diffusive processes are parameterized by an 8th order Shapiro filter.

The islands and straits within the Indonesian archipelago are modeled within the confines of the grid-resolution to give a 4–5 Sv mean throughflow over the upper 300 m, which compares with 6.3 Sv southward baroclinic transport in HG, and a ~7 Sv total transport over the upper 300 m in S98. Observations have yielded a wide range of values with some of the contrast likely explained by interannual variability. Estimates from two current meter moorings in Timor Passage from March 1992 to April 1993 were 4.3 ± 1.0 Sv total-depth mean transport in the strait with 2.5 ± 0.8 Sv over the upper 400 m, Molcard et al. (1996). Murray and Arief (1988), from current meter moorings, estimated a 1.7 Sv mean transport through Lombok Strait, whose sill depth is about 300 m, for 1985. Estimates of Indonesian seas water mass passing through a section between Port Headland, Australia and Bali from data collected during the Java Australia Dynamic Experiment, Fieux et al. (1994), gave a geostrophic plus Ekman transport of 22 ± 4 Sv over the upper 500 m during the southeast monsoon (August) in 1989, but less than a couple of Sverdrups for the northwest monsoon (February) in 1992, Fieux and Molcard (1996). In contrast, Meyers et al. (1995) estimate a net transport of only 5 Sv over the upper

400 m along a repeat XBT line from Shark Bay, Australia to Sunda Strait. In the modeling study presented here, the passages in the archipelago were made narrow enough to give a value on the lower side of observations to contrast with the results of HG and S98.

2.2 Surface heat and salinity fluxes

The surface condition on salinity is effectively a relaxation to the National Oceanographic Data Center's (NODC) climatological monthly sea–surface salinity, as in Levitus et al. (1994). However, instead of prescribing a virtual salinity flux with no change in mass, the natural boundary condition formulation of a fresh-water flux with an associated change in mass is used. The fresh-water flux is calculated as:

$$-\rho_o S \frac{\partial h}{\partial t} = \kappa_S (S_{obs} - S),$$

where h is the depth of the mixed layer and S its salinity, S_{obs} is the observed surface salinity from NODC 1994 climatology, and $\kappa_S = 1/39.9$ kg m^{-2} s^{-1}.

The surface heat flux is evaluated on two grids as in Schopf and Loughe (1995). Firstly, the model's mixed layer temperature is strongly damped with coefficient $\lambda = 100$ Wm^{-2}K^{-1} to observed SST, namely the National Centers for Environmental Prediction's (NCEP) objectively analyzed SST, Reynolds and Smith (1995), on a coarse grid with resolution 4°×5°. Secondly, the model's mixed layer temperature is weakly damped ($\lambda = 25$ Wm^{-2}K^{-1}) to observed SST on the fine-resolution geometry grid of the model. By using the multi-scale approach, the mean SST field in each experiment is constrained to resemble observations, but the fine-scale eddy and frontal structures are more realistically damped. Therefore, in contrasting runs with and without a throughflow, the large-scale surface heat fluxes are expected to be very similar with differences showing up in the finer-scale features.

2.3 Wind stress forcing

Runs are described resulting from forcing the model with two different monthly climatologies. The first product is monthly mean wind stresses derived from ECMWF 1000 mb winds for 1986 to 1992 inclusive; some of these results were described in Wajsowicz and Schopf (2001). Stresses were derived using Large and Pond's (1981) windspeed-dependent drag coefficient formulation.

The second product is monthly mean SSM/I-retrieved wind stresses. The means were constructed from data for years 1988 to 1993 inclusive generated by Dr. S. Chou and colleagues at NASA/GSFC, see Chou et al. (1997). The wind speeds were derived from SSM/I data, and then the directions are assigned using a variational analysis procedure with ECWMF analyses and conventional surface observations, as described in Atlas et al. (1996).

The annual mean wind–stress over the Indian Ocean for the SSM/I and ECMWF products are shown in Fig. 1a,b respectively. Notable differences are the much larger southwestly wind stresses over the Arabian Sea and Bay of Bengal in the ECMWF product.

2.4 Experiments and initial conditions

In the following sections, results from four experiments are presented. The experiments are made up of a combination of either ECWMF or SSM/I wind stresses, and either realistic geometry, or realistic geometry except for a land-bridge isolating the Indian Ocean from the Pacific Ocean, i.e., no Indonesian throughflow. In each experiment, the model was run for 15 years starting from rest with hydrography specified from NODC 1994 climatology, see Levitus and Boyer (1994), and Levitus et al. (1994). As the POSEIDON model has no bottom topography, the deep-ocean temperature and salinity fields were smoothed across the Indonesian archipelago prior to initialization.

In the following discussion, the last five years of the integration for each experiment were averaged to give a monthly climatology. Runs with a throughflow and with a blocked throughflow are identified by the nomenclature: x(IT), x(NoIT), respectively, where x is ECMWF or SSM/I referring to the wind–stress data set forcing the model. The throughflow's effect in the model forced by SSM/I wind stresses is determined by subtracting SSM/I(NoIT) fields from SSM/I(IT) fields, and similarly for the ECMWF-forced model. It is noteworthy that the year-to-year variability in the five years over which the averages were taken is very small compared with the difference in 5-year means between the x(IT) and x(NoIT) experiments, (x = SSM/I, ECMWF).

3 Annual mean response

3.1 Surface circulation and heat flux

Before presenting the effect of the Indonesian throughflow on the annual mean fields for the Indo-Pacific region to compare with those of HG, it is worthwhile contrasting the total fields produced by the two wind stress products in models including a throughflow. The middle panel of Fig. 1a shows the velocity averaged over the upper 50 m in the SSM/I(IT) model. Notable features of the surface circulation are the South Equatorial Current (SEC) flowing westward between about 10°S and 20°S, which is joined by the Indonesian throughflow between 9°S and 12°S. The SEC is the southern limb of an anticyclonic tropical gyre, whose northern limb is the the South Equatorial Countercurrent (SECC). There is a strong northward cross-equatorial western boundary current, which contributes to a weak anticyclonic gyre in the Arabian Sea. In the Bay of Bengal, there are very weak cyclonic and anticyclonic gyres. The SEC bifurcates near the mid-point of the east Madagascan coast, and the southward flow joins that flowing southward along the east African coast to form the Agulhas Current. There is a weak southeastward flow in the interior.

The net surface heat flux, bottom panel of Fig. 1a, is characterised by a broad region in the northwestern basin of net heat flux into the ocean, which is intensified over the region of the Somali Jet. The net heat flux is directed into the ocean until about 15°S. Between 15°S and 35°S in a broad band across the ocean, the ocean heats the atmosphere in the annual mean. There is intense heating of the atmosphere by the ocean over the Agulhas Current and its retroflection and to the south of Madagascar.

The equivalent fields for the ECMWF(IT) model are shown in Fig. 1b. In the ECMWF(IT) model, the Somali Jet is much stronger, but the southern tropical gyre is weaker. The gyres in the Bay of Bengal are stronger, especially the western boundary current off Sri Lanka. Also stronger is the southward flow off Sumatra. In the western equatorial Pacific, the equatorward western boundary currents are stronger. The net heat flux into the ocean is much more intense over the Somali Jet region and in the northern Arabian Sea. It is slightly

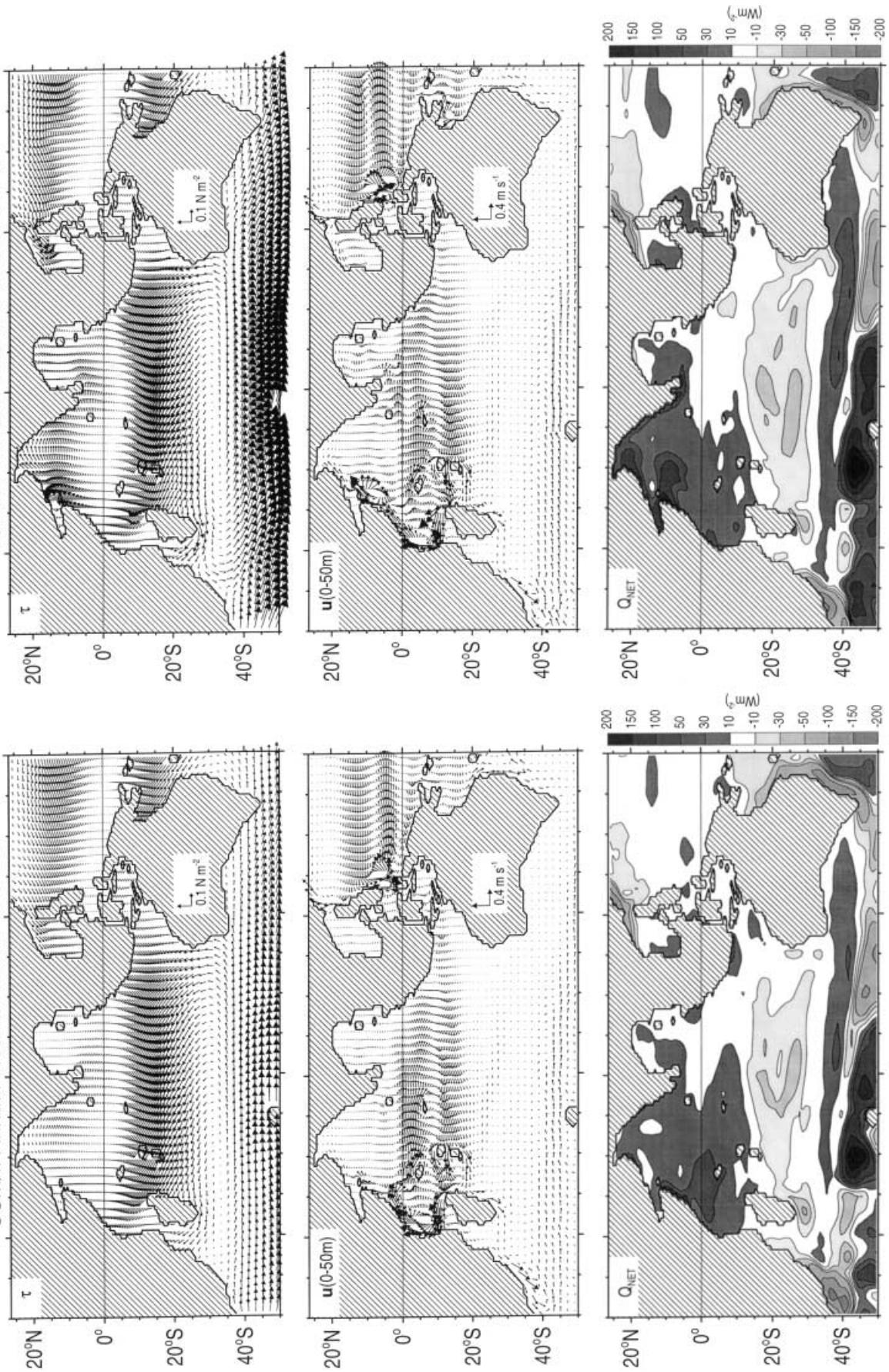

Fig. 1a, b The annual mean wind stress derived from SSM/I wind speeds used to force the global POSEIDON model is shown over the Indian Ocean in the *upper panel* of **a**. The resulting mean ocean currents averaged over the upper 50 m and the net surface heat flux (positive into the ocean) are shown in the *middle* and *lower* panels of **a** respectively. The corresponding fields for the wind – stress product derived from ECMWF 1000 mb winds are shown in **b**. Calibration *vectors* are drawn over Australia, and the contour *scale* is on the *r.h.s.* of the plot

weaker over the western equatorial region. The net surface flux out of the ocean between 10°S and 35°S is stronger, though that over the Agulhas retroflection is typically weaker.

The plots in Fig. 1a,b are for a model with an Indonesian throughflow albeit weak < 5 Sv over the upper 300 m compared to the recent estimates of 1–10 Sv in Makassar Strait (Wajsowicz et al. pers. commun.). The weakness of the modeled throughflow may explain some of the discrepancies between the net surface heat fluxes in Fig. 1a,b and that from observations shown in Fig. 2a from COADS, (da Silva et al. 1994); specifically the large net flux into the atmosphere in the broad region off the west Australian coast, as noted by Godfrey and Weaver (1991). Both wind stress products agree reasonably well with COADS in this region, see upper panel in Fig. 2a. The SSM/I product is typically weaker over the northern Indian Ocean, and the ECMWF product much stronger over the southern region. The lack of a significant net heat flux into the ocean over the southeast Asian seas and over the Bay of Bengal is not obviously attributable to a too weak throughflow. Also shown in Fig. 2b,c are the contributions to the net surface heat flux from latent heating from COADS and SSM/I. SSM/I fluxes derived by Chou et al. (1997) are significantly stronger over the southern tropical Indian Ocean and Arabian Sea. Net surface heat flux estimates are notoriously inaccurate (Glecker and Weare 1997), and so not too much weight should be given to these discrepancies.

3.2 Effect of the Indonesian throughflow

In the coarse-resolution GCM of HG, the throughflow exits the Indonesian seas as a surface-trapped jet, which splits into a broad westward jet along 10°S and a weak southward boundary current along the west Australian coast. It returns eastwards in the surface layers in the Agulhas Current and its retroflection, and in a southeastward current across the ocean interior. The loop is completed by a northward boundary current along the east Australian and New Guinea coasts. The current is intense off southeast Australia due to a recirculation gyre. In HG, the mass in the southeastern interior flow cools and sinks at the southwest corner of Australia, and returns northwestwards to continue the circuit around Madagascar, southward along eastern Africa, across the southern Indian Ocean, and around eastern Australia and New Guinea. Secondary bifurcations occur at the tip of South Africa, and the northern tip of New Guinea. The mass flux, which has sunk into the deeper ocean, is upwelled into upper thermocline over the tropical Pacific Ocean.

A similar surface path for the throughflow, determined by subtracting the x(NoIT) model field from the x(IT) field, is found in both of the POSEIDON models (x = SSM/I, ECMWF) shown in Fig. 3a,b. However, the increased spatial resolution of the numerical grid yields a throughflow jet, which meanders across the Indian Ocean. The velocity fields averaged over the upper 50 m, and between 50 m and 300 m, are shown in Fig. 3 to highlight the baroclinic structure of the distinct eddies, which perturb the zonal jet. The easternmost eddy is the strongest, and makes the surface throughflow apparently bifurcate off Java, so that part of it bends north along the Sumatran coast in the upper 50 m with southward flow below. Differences between the throughflow paths in Fig. 3a,b, include significant northward cross-equatorial flow in the western Indian Ocean and lack of a southward boundary current along northwest Australian coast in the ECMWF-forced model.

The differences in net surface heat flux induced by the throughflow, determined by subtracting the x(NoIT) model field from the x(IT) field (x = SSM/I, ECMWF), are shown in the bottom panels of Fig. 3a, b. Once again, broad features are similar to those found by HG, in particular significant heat gain by the ocean off southeast Australia, and loss to the atmosphere off western Australia and South Africa. The SSM/I- and ECMWF-forced POSEIDON models also have significant net heat loss to the atmosphere over the meandering zonal jet of the throughflow and the southeastward interior flow; HG have only weak net heat loss over these regions. Differences between the SSM/I- and ECMWF-forced models are lack of significant net heat loss to the atmosphere off the northwest Australian coast, but significant net heat loss over the region of the Somali jet, in the ECMWF-forced model. In HG's GCM, the region of heat loss off South Africa extended across the southern Indian Ocean decreasing from about 80 Wm^{-2} to about 15 Wm^{-2} by Australia. In the SSM/I-forced model, the throughflow-induced net surface heat flux is as large a loss to the atmosphere off South Africa as in HG's GCM, but the flux alternates in sign across the southern Indian Ocean. This latter feature is consistent with the climatological meridional temperature gradient and the eddying nature of the throughflow across the southern Indian Ocean in the SSM/I-forced model; where the throughflow is eastwards, or southeastwards, there is heat loss to the atmosphere, as warmer water is advected southwards, but there is a net input into the ocean when the current meanders northwards advecting colder water. In the ECMWF-forced model, where the throughflow has a less eddying character across the southern Indian Ocean, there is a net heat loss to the atmosphere across the region, as found in HG, though it is much weaker. HG actually performed runs with a full throughflow and a purely baroclinic throughflow (comparable to the runs described herein). The latter produced very similar effects to the former, except the surface heat flux difference was about a third less over the Agulhas retroflection, Southern Indian Ocean Current (SIOC) and East Australian Current (EAC), i.e. a similar order to that found in Fig. 3.

HG determined that the throughflow affected the net surface heat flux in regions where convective mixing

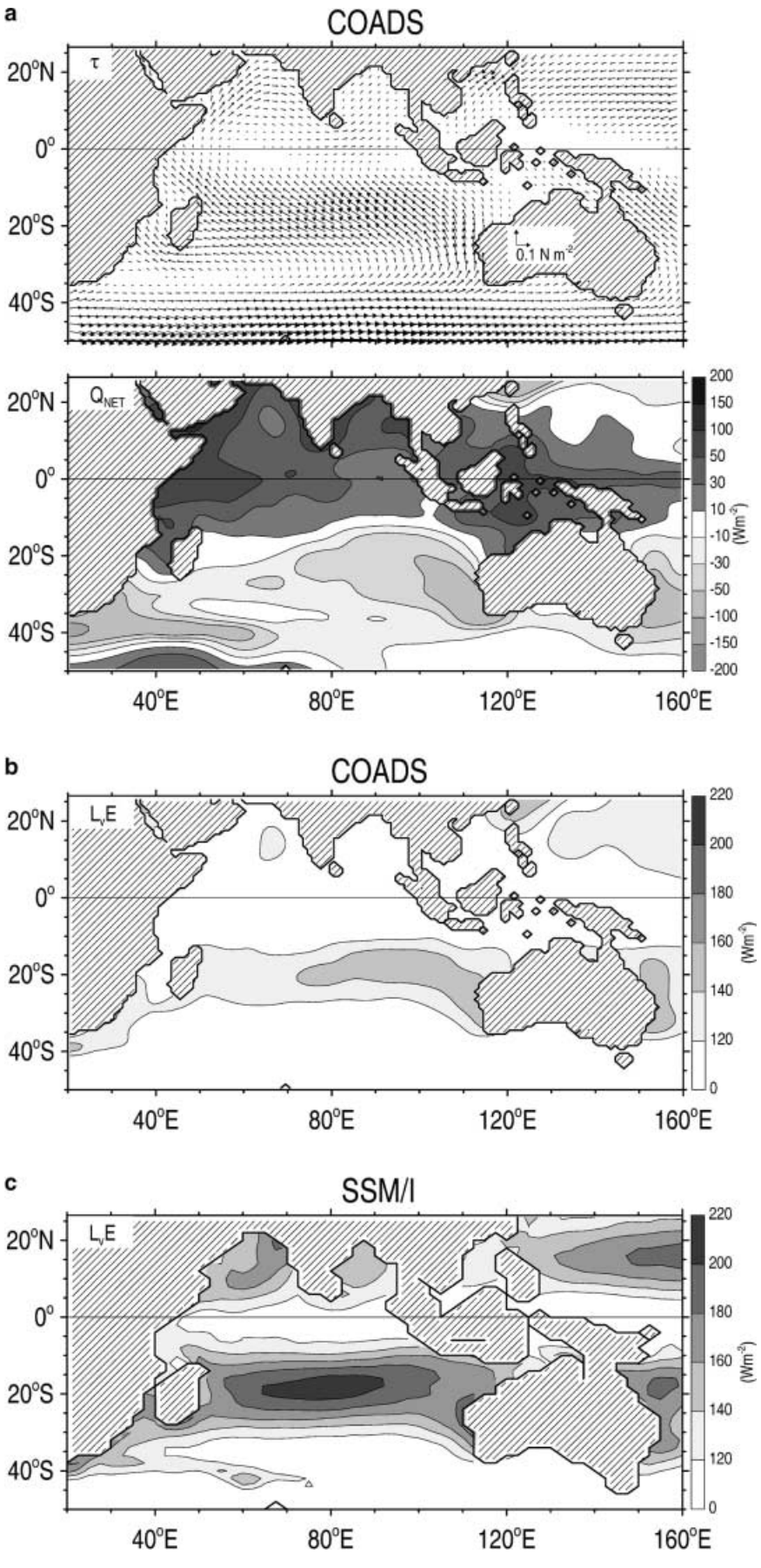

Fig. 2a–c The climatological mean wind stress and net surface heat flux (constrained to be zero over the globe) from COADS are shown in the *upper* and *lower panels* of **a** respectively. The latent heat flux components from COADS and SSM/I data are shown in **b** and **c** respectively

penetrated to the depth of the thermal anomalies associated with the throughflow, e.g., in the southern Indian Ocean Current, and in regions where upwelling brought the anomalies near the surface, e.g., in the equatorial regions. In the SSM/I- and ECMWF-forced POSEIDON models, the same holds true, but as discussed in the next subsection, the throughflow remains more surface-trapped in its path across the Indian Ocean, and hence the greater effect there than found in HG. The reduced effect over the Agulhas retroflection, SIOC and EAC is due to a purely baroclinic throughflow producing much weaker deep temperature anomalies, which are felt by the atmosphere, as the convective mixed layers penetrate to several hundred meters in these regions.

Wajsowicz and Schopf (2001) noted the potential importance of the Indonesian throughflow as a heat source for the southern tropical Indian Ocean enabling it to sustain more vigorous evaporation, which should result in more rainfall somewhere. It is noteworthy that the both wind–stress data sets yield throughflow circulations that produce enhanced heat loss over the southern tropical Indian Ocean, which would likely impact the Indian and east African rainfalls. However, the ECMWF-forced model enhancement over the Somali jet region indicates a further impact on these rainfalls, whereas the SSM/I-forced model enhancement over the exit region off northwest Australia indicates an impact on the rainfall over Indonesia and northern Australia.

3.3 The vertical structure of the Indonesian throughflow

The foregoing description indicates that the vertical structure of the Indonesian throughflow plays a role in determining its effect on the Indian Ocean and overlying atmosphere. The structure of the throughflow in each of POSEIDON's three exit straits, which from west to east are referred to as 'Lombok', 'Savu', and 'Timor' Straits, are shown in Fig. 4 for the upper 300 m. For both wind–stress products, Lombok carries the bulk of the throughflow transport, Timor is next, then Savu. The flow through Lombok Strait is typically warmer and faster at a given depth in the ECMWF(IT) model than in the SSM/I(IT) model, see Fig. 4a. However, the throughflow in the SSM/I(IT) model is more surface-trapped. The temperature decreases with depth for each of the straits shown in Fig. 4a, but the salinity structure is more complex. The very fresh water of the Mindanao Current ($S \sim 33.3$ p.s.u.) is noticeable in Lombok Strait in Fig. 4b. The salinity increases with depth to about 100 m in Lombok Strait; then it decreases slightly. The Lombok flow in the ECMWF(IT) model is fresher, as well as warmer, than that in the SSM/I(IT) model. The flow in the other passages is much more salty, see Fig. 4b.

The passage of the Indonesian throughflow around the Indian Ocean, and the changes in temperature and salinity that it induces with depth, are shown in Fig. 5. The volume transport in the absence of a throughflow (1) along 90°E summed between 20°S and the equator, (2) along the equator summed across the Indian Ocean, and (3) along 35°S summed across the Indian Ocean, are also plotted in Fig. 5a,b using gray shading. Along 90°E, both wind stresses produce similar transport profiles over the upper 300 m averaged between the equator and 20°S. There is a net eastward flow over the upper few tens of meters with westward flow beneath. However, the net transports across the equator and 35°S differ somewhat in magnitude. There is a net northward transport across 35°S in the upper 100 m, which is almost twice as large in the ECMWF(NoIT) model. Below there is a weak southward transport. Across the equator, the transport changes sign several times with depth. It is notably stronger southwards over the upper 20 m in the SSM/I(NoIT) model, but then much stronger southwards in the ECMWF(NoIT) model in the 50–100 m depth range. In the ECMWF(NoIT) model, there is significant northward transport across the equator below 100 m. The contribution that the throughflow makes to these transports is shown in Fig. 5a,b, and with the exception of the near-surface layer across 35°S, is of the same order of magnitude. As well as averages across these sections, averages across the exit straits, i.e., the sum of the transports shown in Fig. 4c, are shown, and also across the entrance straits to the Indonesian archipelago at the latitude of the equator. Notable in both the SSM/I- and ECMWF-forced POSEIDON models is the change in Ekman transport over the archipelago, which induces upwelling, so making the throughflow more surface-trapped, and adds a considerable southward contribution to the near-surface flow. In the SSM/I-forced model, on exiting the archipelago, the near-surface throughflow divides with part continuing as a zonal jet through 90°E, and the remainder turning southwards along the west Australian coast, see Figs. 3a and 5a. Below 50 m, the exit transport continues as a zonal jet through 90°E. In the ECMWF-forced model, there is much less loss to the Leeuwin Current in the near-surface layer, see Fig. 3b and 5b. Between 50 m and about 170 m, some of the westward flow downwells into the layer below. Kundu and McCreary (1986), using a simple single-layer model found that the amount of the transport, which deflected southwards along the west Australian coast, increased with increased vertical mixing. This explanation is consistent with the much larger change in surface heat flux in the exit region found the the SSM/I-forced model shown in Fig. 3a. The thermal anomalies associated with the throughflow at 90°E are O(0.5 °C) in both models, see Fig. 5c, though they are more surface-trapped in the SSM/I-forced model. The throughflow is fresher than the ambient ocean by O(0.1 p.s.u.) with peaks around 50 m, and 150–200 m in the SSM/I-forced model. Consistent with the fresher throughflow shown in Fig. 4b in the ECMWF-forced model, by 90°E, the salinity anomaly is O(-0.2 p.s.u.) and concentrated around 150–200 m, see Fig. 5d.

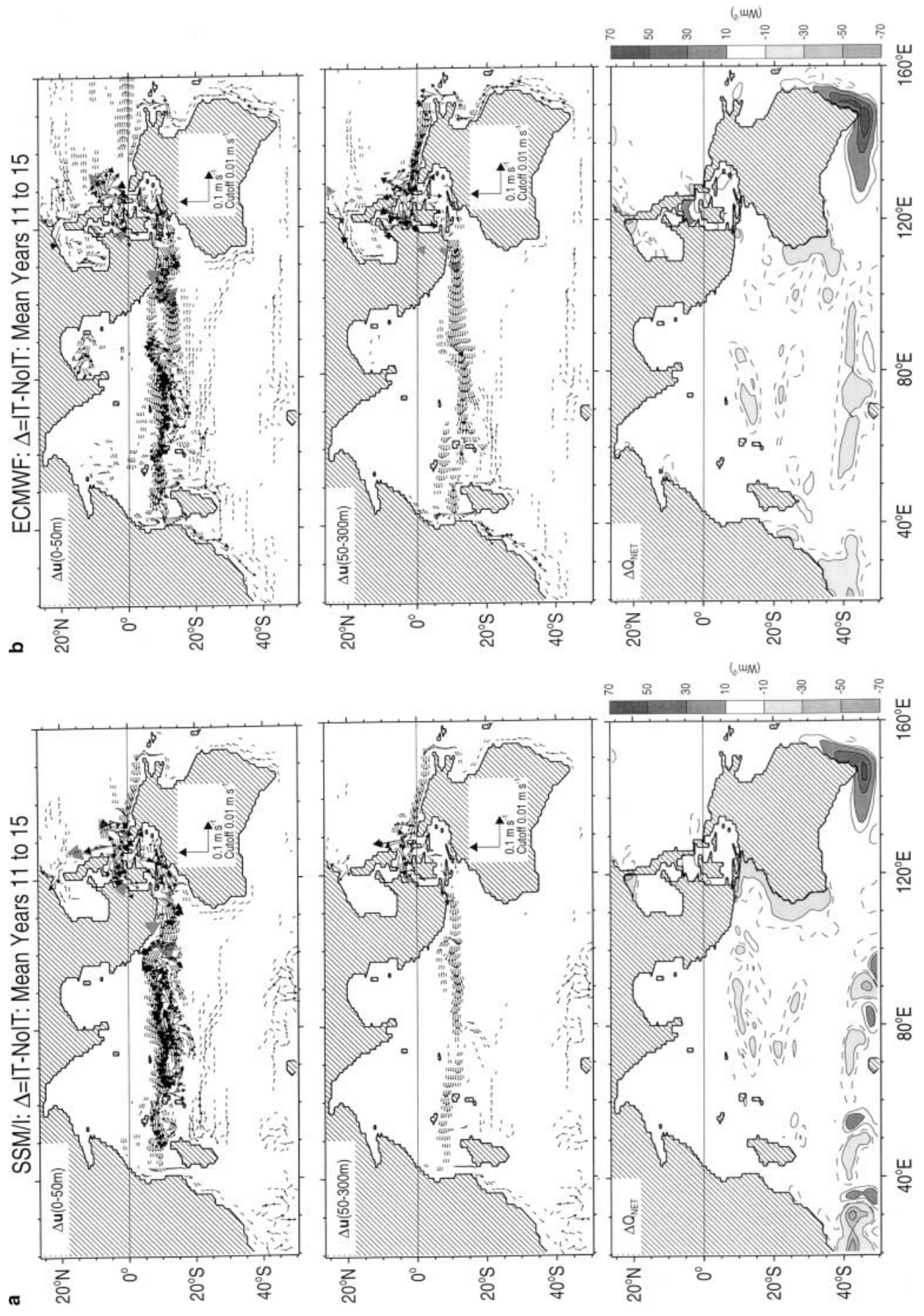
a
SSM/I: Δ=IT-NoIT: Mean Years 11 to 15
b
ECMWF: Δ=IT-NoIT: Mean Years 11 to 15
Δu(0-50m)
Δu(50-300m)
ΔQNET
0.1 m s-1
Cutoff 0.01 m s-1
20°N
0°
20°S
40°S
40°E
80°E
120°E
160°E
(Wm-2)
70
50
30
10
-10
-30
-50
-70

◄

Fig. 3a, b The Indonesian throughflow averaged over the upper 50 m, and between 50 m and 300 m, is shown in the *upper* and *middle panels* of **a** respectively for the SSM/I-forced model, and in **b** for the ECMWF-forced model. The change in net-surface heat flux induced by the throughflow is shown in the *bottom panels* of **a** and **b**. The calibration *vectors* and contour *scales* are drawn over Australia and on the *r.h.s.* of the plot respectively. *Vectors* with amplitudes greater than 0.1 ms^{-1} are *light gray*, and those less than 0.01 ms^{-1} are not drawn. The ± 5 Wm^{-2} contours are denoted by *solid*/*dashed lines* with no shading

The penetration of the throughflow across the equator, inferred from the surface heat flux difference over the Somali Jet region (Fig. 3), is shown in Fig. 5a,b. There is almost no northward transport of the throughflow across the equator, and hence no thermal anomaly, in the SSM/I-forced model above 100 m. In the ECMWF-forced model, though not large, the penetration is sufficient to change the net cross-equatorial transport from south to north above 50 m. Although the surface temperature is strongly relaxed back to observation, which is very effective in the SSM/I-forced model, in the ECMWF-forced model, thermal anomalies induced by the throughflow are still 0.2 °C by 60 m depth, and are as large as 0.8 °C by 170 m, see Fig. 5c. At the equator, the effect of the throughflow on the salinity field is negligible over the upper 150 m, and induces a weak increase in saltiness below, see Fig. 5d.

In the SSM/I- and ECMWF-forced POSEIDON models, the throughflow crosses the Indian Ocean and turns southwards along the east African coast passing to the west of Madagascar; some returns eastwards across the ocean interior, and forms a southward boundary current along the west coast of Australia. By 35°S, the throughflow transport is almost uniform with depth over the upper 300 m in both models, and amounts to about 3 Sv. The maximum thermal anomaly is 0.5 °C between 200 m and 250 m in the ECMWF-forced model, but less than half that in the SSM/I-forced model. Whereas the thermal anomaly induced by the throughflow is always positive, the salinity anomaly varies. At 35°S, the throughflow induces a positive salinity anomaly of about 0.05 p.s.u. in the ECMWF-forced model below 100 m, and about half that in the SSM/I-forced model. HG also found that the salinity anomaly associated with the throughflow was positive by 35°S, which is consistent with You and Tomczak's (1993) tracer analysis. They showed that the throughflow had entrained sufficient surrounding water masses by the time it crossed the Indian Ocean that it could no longer be readily identified.

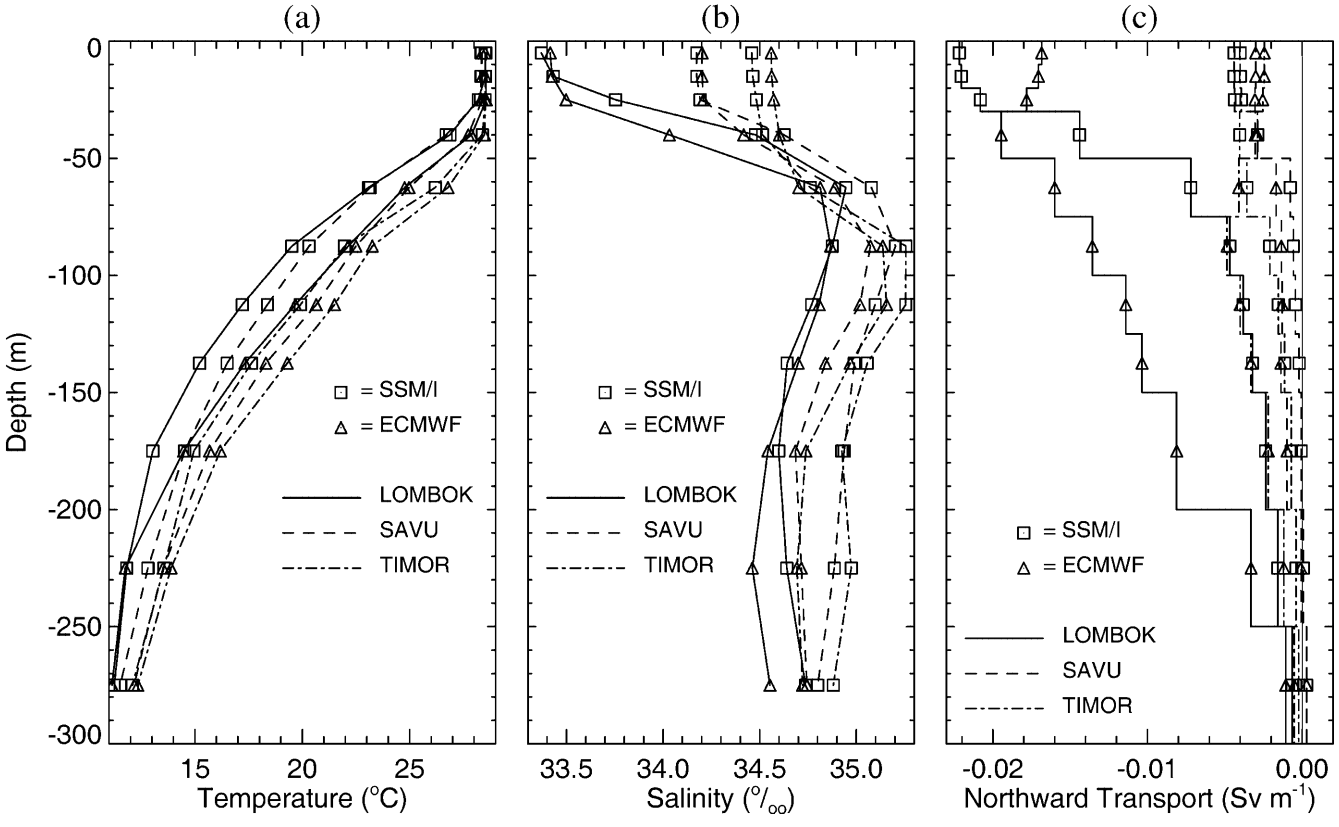

Fig. 4a–c The depth variation in **a** temperature, **b** salinity and **c** volume transport associated with the annual mean throughflow are plotted for models forced by SSM/I and ECMWF wind stresses

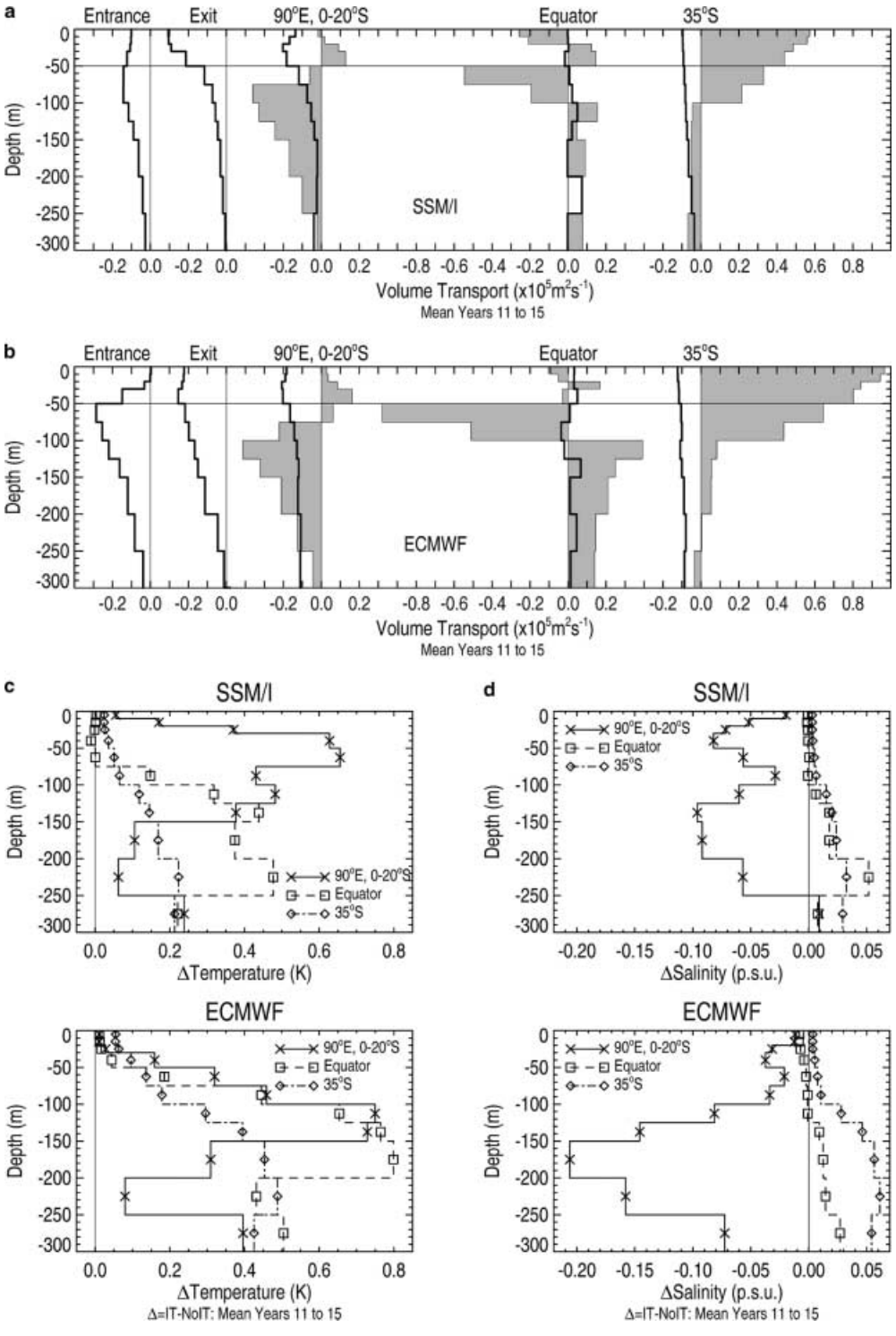

Fig. 5a–d The depth variation in volume transport along sections in the Indian Ocean in the model with a land-bridge blocking the Indonesian archipelago are plotted using *gray shading* for **a** SSM/I-forced model and **b** ECMWF-forced model. The sections are 90°E integrated between the equator and 20°S (*positive* denotes eastwards), along the equator integrated across the basin (*positive* denotes northwards), along 35°S integrated across the basin (*positive* denotes northwards). The modification to the throughflow transport as it crosses these sections, along with its transports at the entrance and exit to the Indonesian archipelago are overplotted using a *bold solid line*. The **c** temperature and **d** salinity perturbations associated with the throughflow averaged along each section are also plotted. Results from the SSM/I-forced and ECMWF-forced models are shown in the *upper* and *lower panels* respectively

4 Seasonal cycle

4.1 Surface circulation and heat flux

The annual harmonic in wind–stress curl has significant amplitude over the equatorial and northern Indian Ocean, and along the west Australian and south Java/Sumatra coasts, see Fig. 6a, and to a lesser degree over the central and western southern Indian Ocean and in a band between 40°S and 50°S. The semi-annual harmonic (not shown) has significant amplitude over the Arabian Sea and to the south of the Agulhas retroflection. Just as the annual mean ECMWF stresses were stronger than those derived from SSM/I data, so are the seasonal components. For both products, the phase of maximum amplitude over the Indian Ocean is January/July for the annual har-

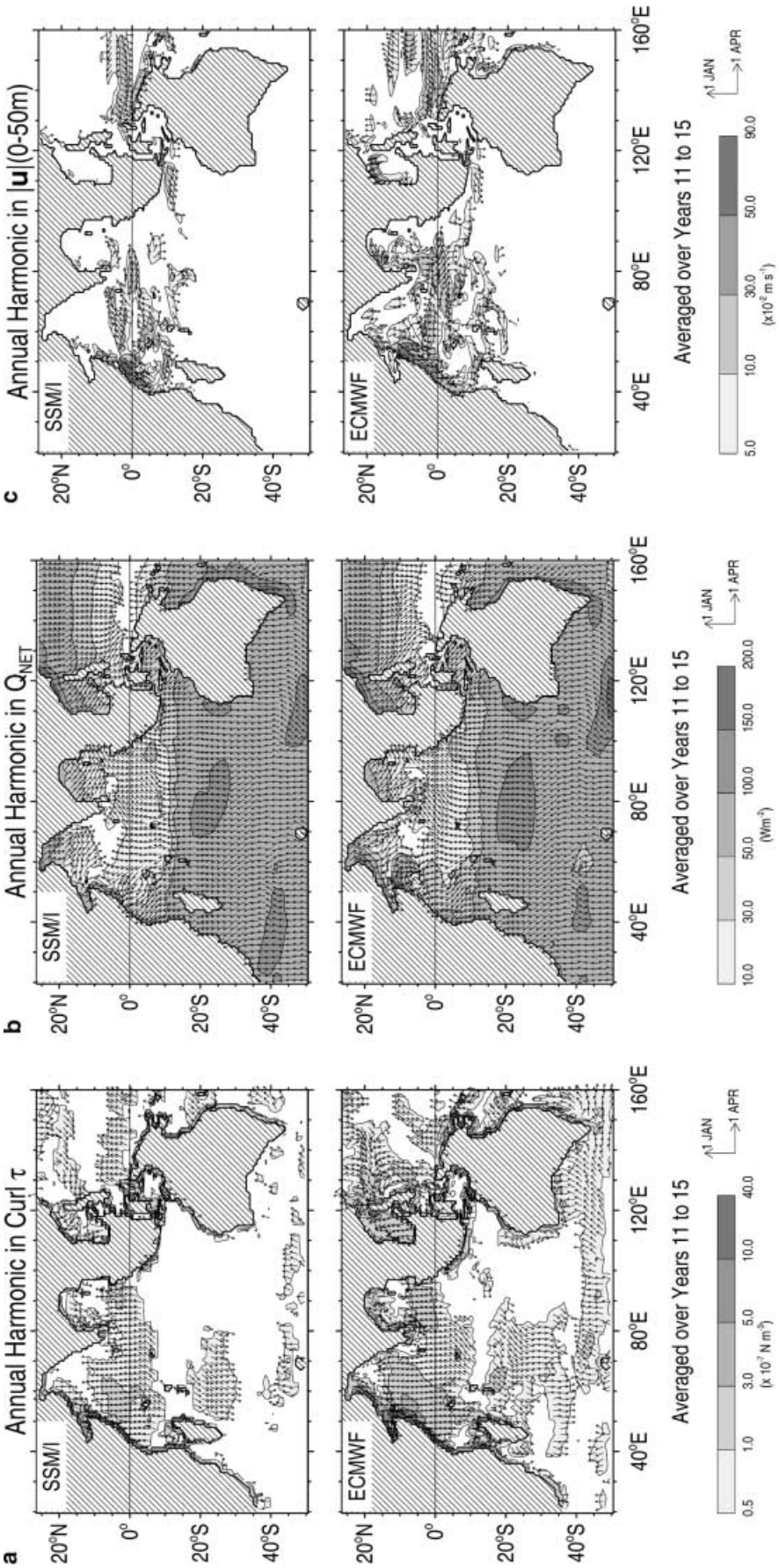

Fig. 6a–c The annual harmonic in **a** wind –stress curl for the SSM/I-derived and ECMWF products over the Indian Ocean are shown in the *upper* and *lower panels* respectively. The annual harmonic in **b** net surface heat flux, and **c** current speed averaged over the upper 50 m from the POSEIDON model when forced by these respective products are shown in the *upper* and *lower panels*. The amplitude is contoured according to the scale at the *bottom* of *each panel*, and the phase is denoted by a clockwise *vector* with a January (April) maximum pointing *north (east)*

monic except for a band centered about 12°S, and off western and southeast Australia, where the phase lags by up to 3 months. The phase of the maximum amplitude for the semi-annual component of the curl (not shown) is April/May over the Somali Jet and its path across the Arabian Sea. At the northern coast, it is January. To the south of the Agulhas retroflection, the maximum amplitude is achieved in February. The resulting net surface heat fluxes in the SSM/I(IT) and ECMWF(IT) models, see Fig. 6b, are very similar with differences confined to the Somali jet region. Both are similar to COADS, but slightly weaker over the southern Indian Ocean, where the amplitude in COADS exceeds 200 Wm^{-2} in several regions. The near-surface circulation, see Fig. 6c, shows the much stronger Somali jet in the ECMWF(IT) model during boreal summer, and the development of flow along the equator in the west in late boreal winter, which reaches into the central region in spring. Both show the peak in flow through the Indonesian archipelago in August. Consistent with the signatures for the annual mean fields shown in Fig. 1, the ECMWF(IT) model shows a much stronger seasonal variability in the Bay of Bengal. The semi-annual signal (not shown) peaks in the equatorial region in April/November with the appearance of the Wyrtki jets.

4.2 Effect of the Indonesian throughflow

The throughflow can be thought to impact the seasonal cycle of net surface heat flux, say, over the Indian Ocean, in two ways. Firstly, seasonal variations in the depth of convective overturning will affect how much the atmosphere feels the warm anomalies due to the mean throughflow. For example, in austral winter, convective overturning in the 40°S to 50°S will be stronger and deeper, and so heat loss to the atmosphere greater. Secondly, the stronger throughflow in boreal summer potentially enables the outflow region to release more heat to the atmosphere. In terms of the path of the seasonal anomalies associated with the throughflow, a change in mass injection should show itself as a coastally trapped Kelvin wave propagating southwards along the west Australian coast. A first baroclinic mode Kelvin wave with wave speed 2.5 ms^{-1} takes only ~20 days to propagate from the exit region to 35°S. As the Kelvin wave propagates southwards part of its energy is scattered into long, westward propagating Rossby waves, see Wajsowicz and Gill (1986). At 10°S, these waves will cross the Indian Ocean in just under a year, at 20°S in three and a half years, and at 35°S in ten years, assuming a width of 60°of longitude. On encountering the western boundary, these waves return equatorward as coastally trapped Kelvin waves, unless a strong southward western boundary current is encountered, which is sufficient to reverse their group velocity.

Figure 7a gives a plan view of the Indonesian throughflow's effect on net surface heat flux; shown is the annual harmonic for the flux field difference x(IT)-x(NoIT), x = SSM/I, ECMWF. The regions affected are similar to those for the mean shown in Fig. 3. This suggests that the effect in part is due to seasonal variations in the depth of the overturning circulation, especially in the 40°S to 50°S band, where the phase is constant with maximum heat input into the ocean in March, three months after the westerlies have peaked. In the region off southeast Australia, the maximum heat input into the ocean is in boreal summer, also three months after the westerlies there have peaked. The amplitude of the annual harmonic in these regions is about 10–20 Wm^{-2}.

Clockwise rotation in the phase vectors along a wave path is indicative of propagation, but this is not evident along the west Australian coast nor in the ocean interior. In fact the phase vectors rotate anticlockwise on moving southwards along the west Australian coast suggesting the effect is related to the march of the solar cycle. Over the ocean interior, the phase vectors are scattered, but typically indicate a maximum heat loss to the atmosphere in boreal summer.

As expected from the effect on the annual mean surface heat flux shown in Fig. 3, SSM/I- and ECMWF-forced models show differences over the Somali Jet and exit region in the east Indian Ocean. In the ECMWF-forced model there is a peak in heat loss to the atmosphere over the Somali Jet in July; the amplitude of the annual harmonic is 10–20 Wm^{-2}. There is also a strong effect, over 40 Wm^{-2}, off the southwest corner of Australia. In the SSM/I-forced model, there is no significant seasonal effect in the northern Indian Ocean, but there is a peak heat loss along the Javan coast in August; the amplitude of the annual harmonic is over 40 Wm^{-2}. The semi-harmonic of the throughflow's effect on the net surface heat flux (not shown) has amplitude O(10 Wm^{-2}). Once again, the regions affected are similar to those of the annual mean. Its phase is directed to give maximum heat loss over the Somali Jet in January/July, over the exit region and 40°S–50°S band in March/October.

The seasonal variation in currents resulting from the presence of the throughflow is plotted in Fig. 7b,c. Over the upper 50 m, propagation of the annual signal along the west Australian coast is evident, though it appears to take nearly three months to reach 35°S from the exit region. This suggests that the wave is a higher order vertical mode, or that it is forced en route rather than being freely propagating. The throughflow affects the ocean currents over the interior in a band between 10°S and 15°S, which extends to about 25°S in the western half of the basin. The phase vectors are scattered in direction, as expected from the eddying nature of the throughflow. However, a group which rotate from April through August on moving from 80°E to 60°E can be distinguished in Fig. 7c and the upper panel of Fig. 7b, which is consistent with a first baroclinic mode Rossby wave.

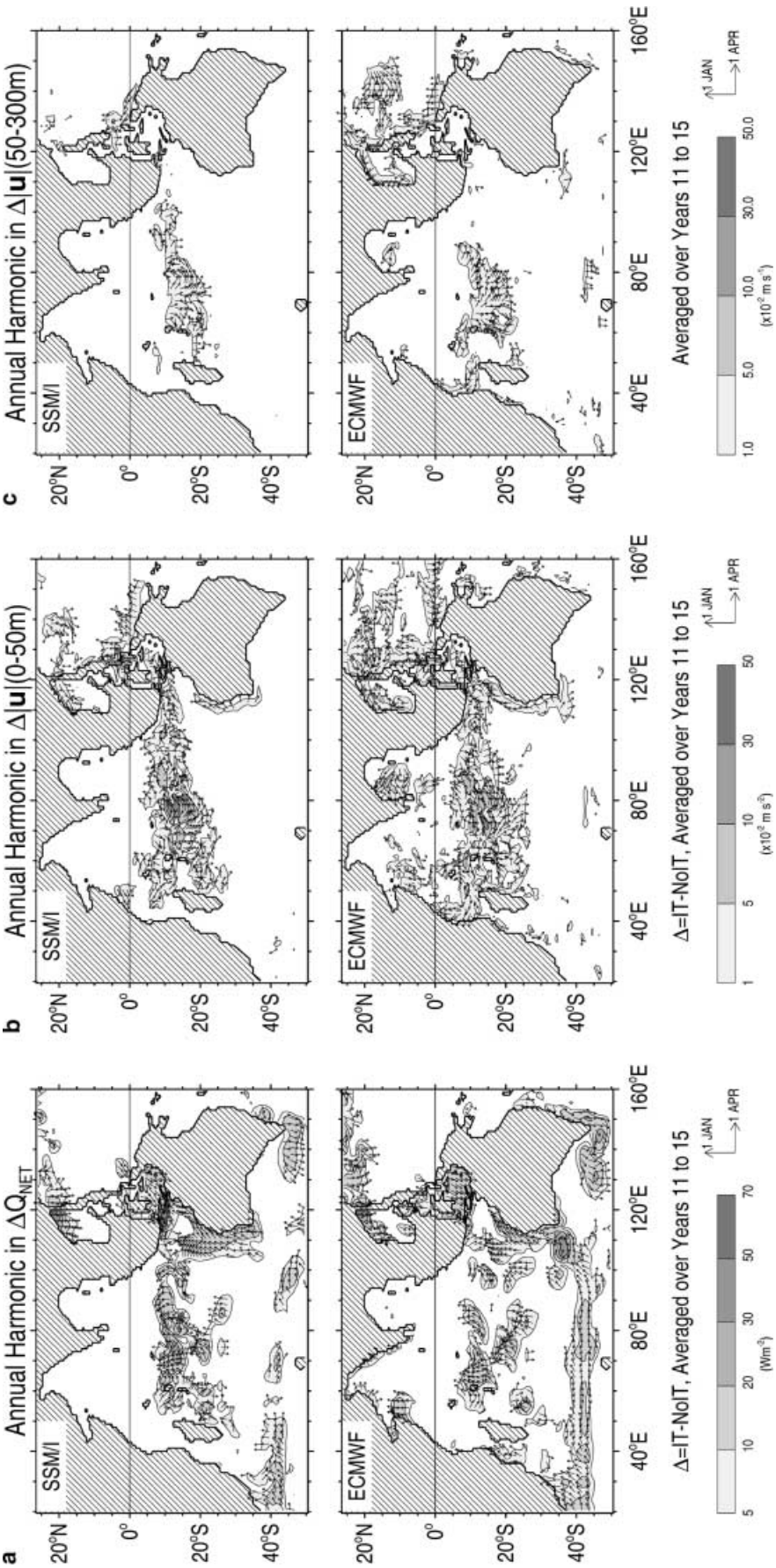

Fig. 7a–c The annual harmonic in **a** net surface heat flux, and current speed averaged over **b** the upper 50 m and **c** between 50 m and 300 m, associated with the Indonesian throughflow, are plotted for the SSM/I- and ECMWF-forced models in the *upper* and *lower panels* respectively. The amplitude is contoured according to the scale at the *bottom* of *each panel*, and the phase is denoted by a clockwise *vector* with a January (April) maximum pointing *north* (*east*)

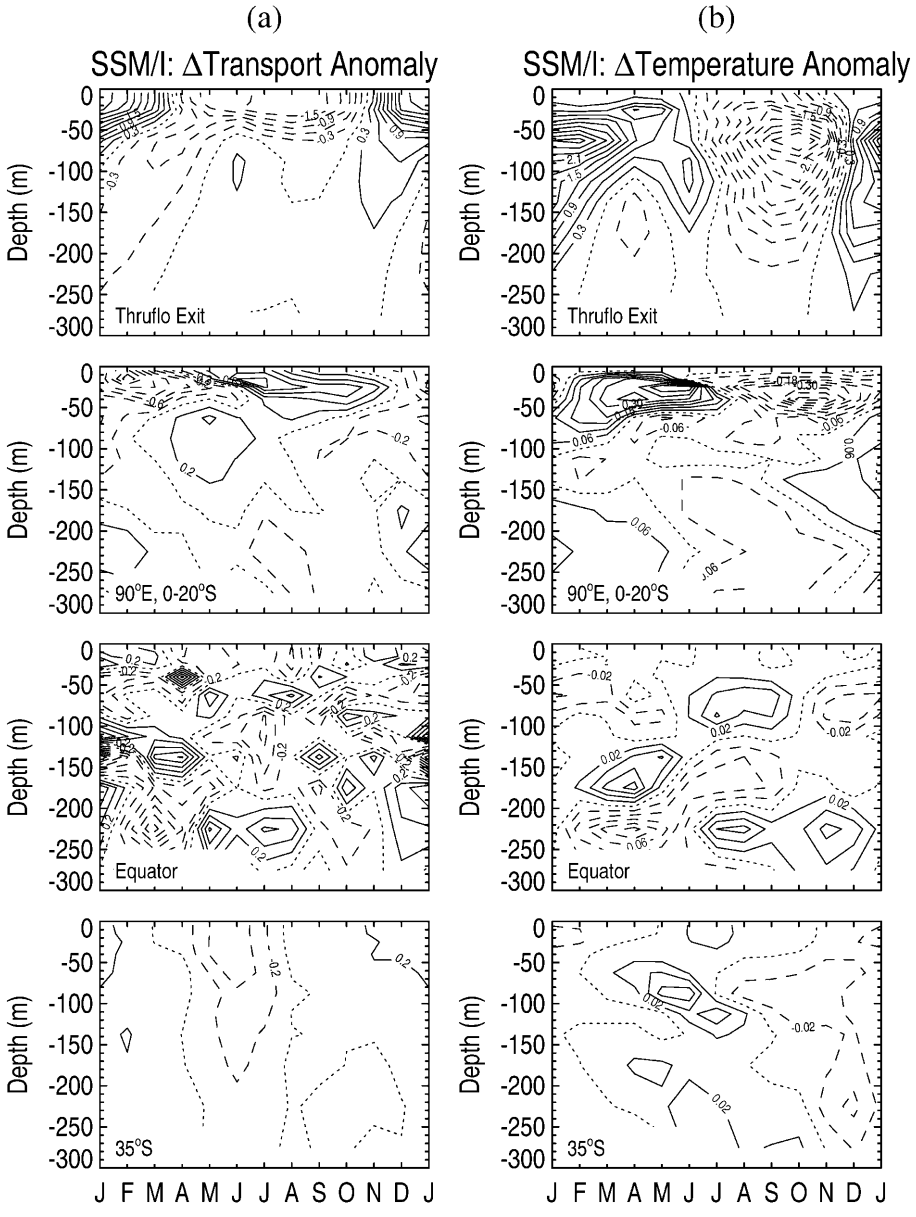

Fig. 8a, b The volume transport anomaly associated with the throughflow in the SSM/I-forced model is contoured in **a** as a function of month and depth for the sum of the channels exiting the archipelago (*upper panel*) and for each of the three sections described in Fig. 5 in descending order. Eastward/northward anomalies are denoted by *solid contours*, the zero contour by a *dotted line*, and westward/southwards anomalies by a *dashed contours*. The contour intervals from *top* to *bottom* are 0.3, 0.2, 0.2, 0.2 $\times$ $10^6 m^2 s^{-1}$. The associated temperature anomalies are shown in **b**. The contour intervals from *top* to *bottom* are 0.3, 0.06, 0.02, 0.02 K, with *positive* (*negative*) anomalies denoted by *solid* (*dashed*) contours, and the zero contour by a *dotted line*

4.3 Vertical structure of the anomalies induced by the throughflow

The anomalies are better assessed by considering the averages along the sections described in Sect. 3.2. At the exit into the east Indian Ocean, in the SSM/I-forced model, the seasonal anomaly in throughflow transport is surface-trapped with a northward maximum in January and a southward maximum extending from July to September, see Fig. 8a. By 90°E, the anomalies have become even more surface trapped with a relative phase lag of six months, consistent with the time taken for first baroclinic mode Rossby waves to propagate from 120°E to 90°E. The corresponding temperature anomalies are shown in Fig. 8b; those at the 'Exit' are just the seasonal anomalies in temperature found in the exit channels around 10°S. A cold anomaly starts in July, which peaks at 3 K in October; it extends over the upper 200 m with the maximum at 60 m. The anomaly rapidly changes sign in December and peaks at 3 K in February. The temperature anomaly is rather weak from April through June. At 90°E, the temperature anomaly is similarly signed to that in the exit channels lagged by about one month, but only about one-seventh the amplitude and confined to the upper 60 m. The lack of agreement in phase between the transport and temperature anomalies induced by the throughflow at 90°E indicates that the temperature anomaly arises from an interaction between the mean throughflow and the seasonal cycle of the Indian Ocean circulation. In the SSM/I-forced model, the transport signal crossing the equator is very noisy. The temperature anomalies are more coherent, but deep and weak < 0.1 K, see Fig. 8b. By 35°S, the transport anomaly is almost an order of magnitude smaller than in

the exit channels. It is southward from May through July, and northward the rest of the year. There are weak subsurface temperature anomalies, which are positive during boreal summer and negative otherwise.

In the ECMWF-forced model, the vertical structure of the seasonal transport anomalies in the exit channels is somewhat different from that in the SSM/I-forced model, see Fig. 9a and compare with Fig. 8a. The structure above 50 m is similar, but the anomalies below are much enhanced resulting in subsurface maxima and significant opposite-signed anomalies at depth over much of the year. The temperature anomaly, shown in the top panel of Fig. 9b, is similar to that shown in Fig. 8b in vertical structure, but slightly weaker. At 90°E, the transport anomaly is essentially confined to the upper hundred meters. It is typically out-of-phase with exit signal, and has become notably fragmented. The corresponding temperature anomaly is almost zero above 50 m with a strong semi-annual signal in the 50–150 m depth range. Across the equator, the transport anomaly signal is similarly noisy except for a very strong northward anomaly at the surface in August due to the very strong northward ECMWF wind stresses associated with the Findlater Jet. Once again, there is no temperature signal near the surface, but significant anomalies between 50 m and 150 m. The transport and temperature anomalies averaged across 35°S are similar to those in the SSM/I-forced model, but almost twice as large.

5 Summary and discussion

The effect of the Indonesian throughflow on the circulation of the upper thermocline and net surface heat flux over the Indian Ocean has been explored using a quasi-

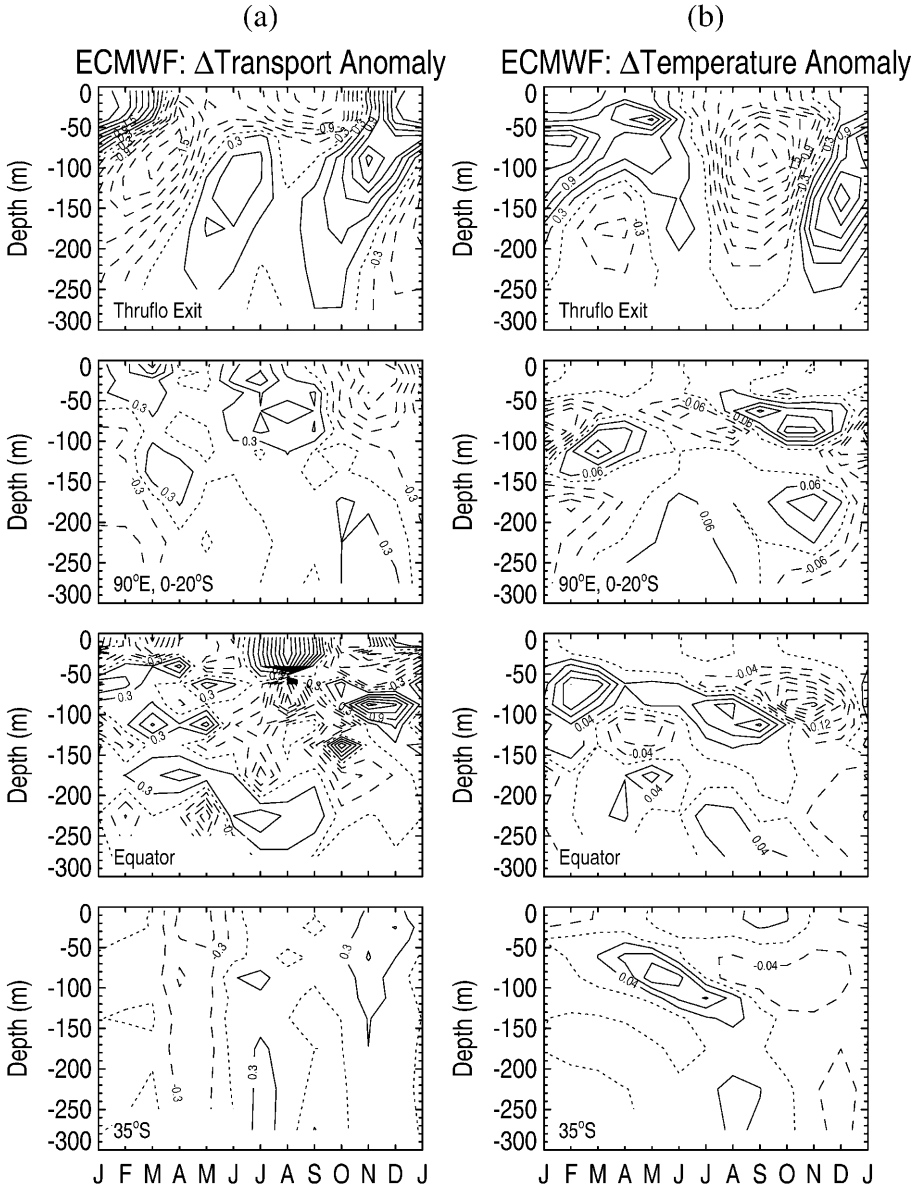

Fig. 9 a, b As in Fig. 8, but for the ECMWF-forced model

isopycnal, multi-layer, reduced-gravity model, POSEIDON forced by two different wind–stress products. There are significant differences between the effects in each model. In the SSM/I-forced model, the exiting throughflow splits in two. Part continues as a meandering, zonal jet across the Indian Ocean, and the remainder is deflected southwards along the west Australian coast; in the ECMWF-forced model, almost all continues westwards. The amount deflected along the Australian coast depends on the amount of vertical mixing, as described by Kundu and McCreary (1986). In the east Indian Ocean surrounding the exit latitudes of the throughflow, the ambient Ekman transport is opposed to that of the throughflow, which is south turning west. The transport within the mixed layer in the SSM/I-forced model is about 50% greater than that in the ECMWF-forced model due to differences in the wind stresses over the Pacific Ocean and Indonesian seas. On entering the Indian Ocean, therefore, a greater adjustment is required in the SSM/I-forced model, which results in a greater output of heat to the atmosphere, as the incoming surface flow cools and sinks. In the exit region, the throughflow induces an increase in heat output to the atmosphere of 10–30 Wm^{-2} in the SSM/I-forced model; it peaks at nearly 50 Wm^{-2} at the site of the land-bridge. The main thermal anomaly associated with the throughflow is much closer to the surface in the SSM/I-forced model, as it crosses the Indian Ocean. Hence, it is more readily sensed by the atmosphere, and the net surface heat flux anomaly is larger in this model over the meandering zonal jet.

In the absence of a throughflow, there is a much stronger mean southward Ekman transport across the equator in the SSM/I-forced model than in the ECMWF-forced model. Hence, in the SSM/I-forced model, less of the throughflow signal penetrates the northern Indian Ocean, where the throughflow temperature anomaly is sensed by the atmosphere over the Somali Jet, as upwelling brings the signal nearer to the surface. In the ECMWF-forced model, the net heat output to the atmosphere in the annual mean is O(10 Wm^{-2}) over the Somali Jet. Over the extended Leeuwin Current system, described in HG as a southeastward upper layer flow across the interior of the Indian Ocean, which sinks at the southwest corner of Australia, and returns northwestwards at depth, both models have an O(10 Wm^{-2}) throughflow-induced heat output to the atmosphere.

Along its path southwards through the Indian Ocean, and eastwards into the Pacific, the atmosphere next senses the mean throughflow over the Agulhas retroflection and south Indian Ocean Current, where convective mixing extends over several hundred meters. As described in HG, the effect is much weaker over these latitudes for a purely baroclinic throughflow, and as seen in the SSM/I-forced model, horizontal advection may dominate yielding a +/- pattern in response to the meandering throughflow. Both models have a strong throughflow-induced heat input into the ocean over the south Tasman Sea; the peak is nearly 100 Wm^{-2}. As in HG, this is attributed to advection of colder water from the south by the throughflow, which forms a western boundary current along the east Australian coast. In the absence of a throughflow, the East Australia Current (EAC) advects warm water southwards into this region, but in the run with a throughflow, the EAC separates from the coast at about 30°S permitting the throughflow to enter the region.

At first sight, it is remarkable that the throughflow's effect on net surface heat flux in the annual mean is very similar in magnitude to that found in Hirst and Godfrey (1993) and Schneider (1998) for a throughflow about three times as large. However, on considering the processes by which the throughflow affects the surface heat flux, the implication is that in all of the models, the throughflow has a similar transport and temperature over the upper 50 m, and that the differences occur at depth.

Regarding seasonal variability in the throughflow's effect on the Indian Ocean circulation and its air–sea interaction, the results suggest that the seasonal variability in the throughflow itself is not important except in the exit region. In general, the effects mimic those of the annual mean indicating that it is the seasonal variability of the Indian Ocean circulation and changes in the strength of convective overturning and advection acting on the mean throughflow thermal anomalies, which produce the observed effects, see Schneider (1998). Interestingly, the mean, annual harmonic and semi-annual harmonic add to give peak throughflow-induced net surface heat flux in boreal summer. In the SSM/I-forced model, the net heat output to the atmosphere exceeds 40 Wm^{-2} over patches of the extended Leeuwin Current system, and exceeds 60 Wm^{-2} over the Agulhas retroflection and immediate exit region of the throughflow in the eastern Indian Ocean. Similar values are obtained in the ECMWF-forced model, except inthe exit region where there is little effect. Instead, there is a 30 Wm^{-2} output to the atmosphere over the Somali jet in boreal summer.

The effect of seasonal variations in the throughflow is apparent to the south of Java, where there is a thin wedge of net surface heat flux difference with a maximum into the ocean in boreal summer. This is consistent with the cool seasonal anomaly in exiting temperature. Adjacent to this region to the south, there is a wedge of heat flux anomalies, which are a maximum into the atmosphere in boreal summer. This effectively extends a similarly phased region along Australia's west coast well into the interior ocean with the westward extent of the region determined by how far annual period Rossby waves propagate before decaying.

Acknowledgements This research was funded by NASA Grant NAG53960, and the computations were carried out on the CRAY at NASA/Goddard Space Flight Center Supercomputer Facility. Partial support was also provided by ONR grant N000149610611. The author would like to thank Drs. S.-H. Chou and C.-L. Shie of the Mesoscale Atmospheric Processes Branch at NASA/Goddard Space Branch for providing the air–sea fluxes used in this research, which were derived in part using data provided by Dr. R. Atlas and J. Ardizzone of the Data Assimilation Office at NASA/Goddard

Space Flight Center. She would also like to thank Prof. P.S. Schopf of George Mason University for his help in setting up the POSEIDON model developed at NASA/Goddard Space Flight Center. The author is also affiliated with the Earth System Science Interdisciplinary Center, University of Maryland at College Park.

References

Atlas R, Hoffman RN, Bloom SC, Jusem JC, Ardizzone J (1996) A multiyear global surface wind velocity dataset using SSM/I wind observations. Bull Am Meteorol Soc 77: 869–882

Chou S-H, Shie C-L, Atlas RM, Ardizzone J (1997) Air–sea fluxes retrieved from Special Sensor Microwave Imager data. J Geophys Res 102: 12705–12726

da Silva A, Young C, Levitus S (1994) Atlas of Surface Marine Data 1994, vol 1, Algorithms and procedures. NOAA Atlas NESDIS 6, US Government Printing Office, Washington DC, USA 83pp

Fieux M, Molcard R (1996) Geostrophic transport of the Pacific–Indian Oceans throughflow. J Geophys Res 101: 12421–12432

Fieux M, Andrie C, Delecluse P, Ilahude AG, Kartavtseff F, Mantisi R, Molcard R, Swallow JC (1994) Measurements within the Pacific–Indian oceans throughflow region. Deep–Sea Res Part 1 41: 1091–1130

Glecker PJ, Weare BC (1997) Uncertainties in global ocean surface heat flux climatologies derived from ship observations. J Clim 10: 2764–2781

Godfrey JS, Weaver AJ (1991) Is the Leeuwin Current driven by Pacific heating and winds? Prog Oceanogr 27: 225–272

Gordon AL, Susanto RD, Ffield A (1999) Throughflow within Makassar Strait. Geophys Res Lett 26: 3325–3328

Hirst AC, Godfrey JS (1993) The role of the Indonesian throughflow in a global ocean model. J Phys Oceanogr 23: 1057–1086

Hsiung J (1985) Estimates of global oceanic meridional heat transport 1985. J Phys Oceanogr 15: 1405–1413

Kundu PK, McCreary JP (1986) On the dynamics of the throughflow from the Pacific into the Indian Ocean. J Phys Oceanogr 16: 2191–2198

Large WG, Pond S (1981) Open ocean momentum flux measurements in moderate to strong winds. J Phys Oceanogr 11: 324–336

Levitus S, Boyer TP (1994) World Ocean Atlas 1994, vol 4: temperature. NOAA Atlas NESDIS 4,US Government Printing Office, Washington, DC, USA, 117pp

Levitus S, Burgett R, Boyer T (1994) World Ocean Atlas 1994, vol 3: Salinity. NOAA Atlas NESDIS 3,US Government Printing Office, Washington, D.C., USA 99pp

Meyers G, Bailey RJ, Worby AP (1995) Geostrophic transport of the Indonesian throughflow. Deep-Sea Res Part 1 42: 1163–1174

Molcard R, Fieux M, Ilahude AG (1996) The Indo–Pacific throughflow in the Timor Passage. J Geophys Res 101: 12411–12420

Murray SP, Arief D (1988) Throughflow into the Indian Ocean through Lombok Strait, January 1985–January 1986. Nature 333: 444–447

Reynolds RW, Smith TM (1995) A high resolution global sea surface temperature climatology. J Clim 8: 1572–1583

Schneider N (1998) The Indonesian throughflow and the global climate system. J Clim 11: 676–689

Schopf PS (1994) Documentation of the POSEIDON Ocean Model Version 4. NASA/Goddard Space Flight Center Techn Rep 211 pp

Schopf PS, Loughe A (1995) A reduced gravity isopycnal model – hindcasts of El Nino. Mon Weather Rev 123: 2839–2863

Talley LD (1984) Meridional heat transport in the Pacific Ocean. J Phys Oceanogr 14: 231–241

Wajsowicz RC, Gill AE (1986) Adjustment of the ocean under buoyancy forces. Part 1: the role of Kelvin waves. J Phys Oceanogr 16: 2097–2114

Wajsowicz RC, Schopf PS (2001) Oceanic influences on the seasonal cycle in evaporation rate over the Indian Ocean. J Clim 14: 1199–1226

You Y, Tomczak M (1993) Thermocline circulation and ventilation in the Indian Ocean derived from water mass analysis. Deep-Sea Res Part 1 40: 13–56